CrossMark

Confocal Annular Josephson Tunnel Junctions with Large Eccentricity

Roberto Monaco[1] · **Jesper Mygind[2]** ·
Lyudmila V. Filippenko[3]

Abstract Confocal annular Josephson tunnel junctions (CAJTJs), which are the natural generalization of the circular annular Josephson tunnel junctions, have a rich nonlinear phenomenology due to the intrinsic non-uniformity of their planar tunnel barrier delimited by two closely spaced confocal ellipses. In the presence of a uniform magnetic field in the barrier plane, the periodically changing width of the elliptical annulus generates a asymmetric double-well for a Josephson vortex trapped in a long and narrow CAJTJ. The preparation and readout of the vortex pinned in one of the two potential minima, which are important for the possible realization of a vortex qubit, have been numerically and experimentally investigated for CAJTJs with the moderate aspect ratio 2:1. In this work, we focus on the impact of the annulus eccentricity on the properties of the vortex potential profile and study the depinning mechanism of a fluxon in more eccentric samples with aspect ratio 4:1. We also discuss the effects of the temperature-dependent losses as well as the influence of the current and magnetic noise.

✉ Roberto Monaco
  r.monaco@isasi.cnr.it

  Jesper Mygind
  myg@fysik.dtu.dk

  Lyudmila V. Filippenko
  lyudmila@hitech.cplire.ru

[1] CNR-ISASI, Institute of Applied Sciences and Intelligent Systems "E. Caianello", Comprensorio Olivetti, 80078 Pozzuoli, Italy

[2] DTU Physics, B309, Technical University of Denmark, 2800 Lyngby, Denmark

[3] Kotel'nikov Institute of Radio Engineering and Electronics, Russian Academy of Sciences, Mokhovaya 11, Bldg 7, Moscow, Russia 125009

🙋 Springer

1 Introduction

The problem of a particle in a double-well potential (DWP), characterized by two adjacent—in general unequal—potential minima, is almost as old as quantum mechanics [1], and one of the first applications was the calculation of an inversion frequency of the ammonia molecule back in 1932 [2]. During the last two decades, the phenomenon of tunneling in asymmetric DWPs was actively considered across several branches of physics and found application in the study of systems, such as the Bose–Einstein condensates in trapped potentials [3–7] and the quantum superconducting circuits based on of low-capacitance Josephson tunnel junctions (JTJs) [8–12]. The latter have attracted great attention due to their potential use as elementary bits of quantum information (qubits, i.e., two-state quantum-mechanical systems) capable of implementing quantum computing operations.

Long and narrow, annular JTJs are potential qubit candidates due to their unique capability to trap a Josephson vortex (a supercurrent loop carrying one magnetic flux quantum also called fluxon) whose center of mass becomes the macroscopic collective coordinate of a massive particle: At sufficiently small temperatures, the particle enters the quantum regime as it shows discrete energy levels within a potential well [13] and can escape from a potential well via macroscopic quantum tunneling [14]. Different techniques have been adopted to implement a two-minima fluxon potential in a long JTJ by the application of an external magnetic field and/or on some abrupt changes in the tunnel barrier properties, either the curvature radius [14] or the Josephson current density [15,16]. An alternative approach has been proposed [17] which takes advantage of the proportionality between the fluxon spatial potential and the local width of the long JTJ [18]. It follows that a large variety of spatially dependent fluxon potentials can be engineered by means of JTLs having a non-uniform width [19]. In particular, a magnetically tunable double-well potential was conjectured in a variable-width annular JTL named confocal annular Josephson tunnel junction (CAJTJ) [20] where the tunneling area is delimited by two ellipses having the same focal length. Figure 1 shows the scanning electron microscope image of a CAJTJ made of *Nb* doubly connected electrodes. The CAJTJs represent a generalization of the well-known circular (i.e., zero-eccentricity) annular JTJs intensively studied to experimentally test the perturbation models developed to take into account the dissipative effects in the propagation with no collisions of sine-Gordon kinks [21–23] and to investigate both the static and the dynamic properties of a fluxon in the spatially periodic potential induced by an in-plane magnetic field [24–26]. At variance with the ring-shaped JTLs which have a constant width, it is seen that for the CAJTJs the width of the planar tunnel barrier is smallest at the equatorial point and largest at the poles; the width variation is smoothly distributed along one fourth of the elliptical annulus (mean) perimeter. It is this smooth periodic change of the width of the planar tunnel barrier that makes the physics of CAJTJs very rich and interesting especially since the modeling is very accurate [20,27]. Recently [28], experiments have shown that a fluxon trapped in a

Fig. 1 Scanning electron microscope image of a confocal annular Josephson tunnel junction (CAJTJ) made of Nb doubly connected electrodes. The ratio of the major axis and the minor axes is 2:1 that implies that the equatorial annulus width is one half of the polar width
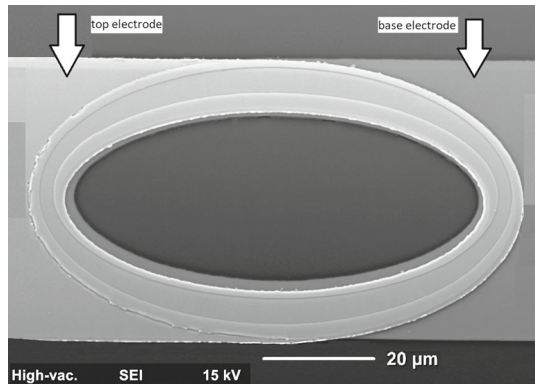

long and narrow CAJTJ experiences a finely tunable DWP and both the preparation and readout of the vortex states in either the left or right state, that are important with respect to the possible realization of a vortex qubit, can be achieved by simple and robust procedures. The previously presented findings concerned CAJTJs with the moderate aspect ratio of 2:1 in which, as in Fig. 1, the (mean) major diameter is twice larger than the minor one. In this paper, we investigate the effect of the annulus eccentricity on the properties of the intrinsic fluxon DWP and present both numerical and experimental findings on CAJTs with aspect ratio of 4:1. In particular, we will focus on the mechanisms influencing the depinning of a fluxon from each of the potential wells.

The paper is organized into five sections. Section 2 introduces the theoretical framework for the study of a current-biased CAJTJ subjected to an external magnetic field in a modified and perturbed sine-Gordon equation; we then consider the two-minima periodic potential experienced by a trapped fluxon and discuss how the potential changes with the system aspect ratio and how it can be tuned by means of an external in-plane magnetic field and/or bias current. In Sect. 3, we present numerical simulations of the depinning of a fluxon from each of the two stable states of the DWP in underdamped CAJTJs and describe a protocol to reliably prepare and determine the vortex state. In Sect. 4, we present the experimental data obtained with high-quality low-loss Nb/Al-AlO$_x$/Nb window-type CAJTJs in the presence of in-plane magnetic fields and discuss the role of the temperature and noise on the fluxon depinning. The conclusions of our work are presented in Sect. 5.

2 Theory of One-Dimensional CAJTJs

The tunneling area of two CAJTJs with different aspect ratios is sketched by the hatched area in the top panels of Fig. 2a, b where the principal diameters of the confocal ellipses are made parallel to the X and Y axes of a Cartesian coordinate system. The common foci (small gray closed circles) lie on the X-axis at $(\pm c, 0)$. As the focal points move toward the origin, the eccentricity vanishes and the confocal annulus progressively reduces to a circular annulus (with uniform width).
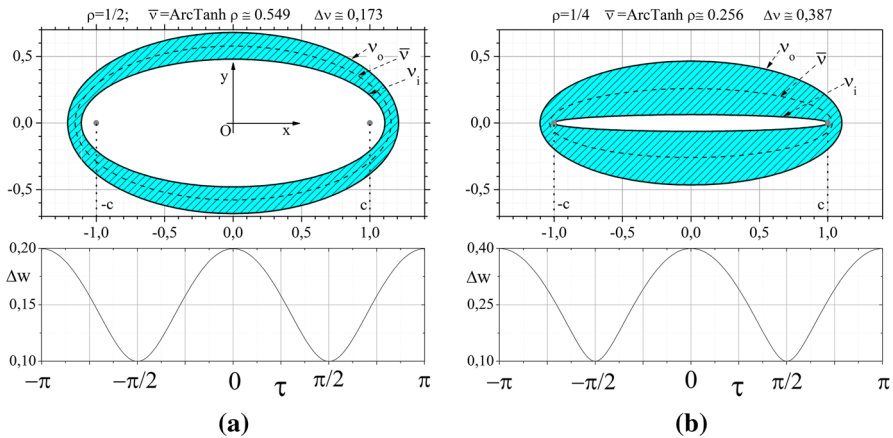
Fig. 2 Top panels: drawings of two confocal annuli delimited by closely spaced confocal ellipses (hatched area) identified by the radial elliptic coordinates ν_i and ν_o; they represent the tunneling areas of two CAJTJs having the same foci—the gray dots at $(\pm 1, 0)$, but different aspect ratios, ρ,: **a** $\rho = 1/2$, $\nu_o \approx 0.6358$ and $\nu_i \approx 0.4628$ and **b** $\rho = 1/4$, $\nu_o \approx 0.4495$ and $\nu_i \approx 0.0625$. The dashed line locates one more confocal ellipse, called mean or master ellipse as $\bar{\nu} \equiv (\nu_o + \nu_i)/2$. The annuli are built to have the same equatorial or minimum width, $\Delta w_{\min} = c \sinh \bar{\nu} \, \Delta \nu = 0.1$, with $\Delta \nu \equiv \nu_o - \nu_i$. Bottom panels: the annuli width, Δw, varies with the angular elliptic coordinate, τ, as given by (1) (Color figure online)

The geometry of our system suggests the use of the (planar) elliptic coordinate system (ν, τ), a two-dimensional orthogonal coordinate system in which the coordinate lines are confocal ellipses and hyperbolae. In this system, any point (x, y) in the X-Y plane is uniquely expressed as $(c \cosh \nu \sin \tau, c \sinh \nu \cos \tau)$ with $\nu \geq 0$ and $\tau \in [-\pi, \pi]$ for a given positive c value. According to these notations, the origin of τ lies on the positive Y-axis and increases for a clockwise rotation. In the limit $c \to 0$, the elliptic coordinates (ν, τ) reduce to polar coordinates (r, θ), where θ is the angle relative to the Y-axis; the correspondence is given by $\tau \to \theta$ and $c \cosh \nu \to r$ (note that ν itself becomes infinite as $c \to 0$). Each possible ellipse with focal points in $(\pm c, 0)$ is uniquely identified by a value of ν; we will name ν_i and $\nu_o > \nu_i$ the characteristic values of, respectively, the inner and outer elliptic boundaries of a CAJTJ. Their mean value, $\bar{\nu} = (\nu_o + \nu_i)/2$, labels one more confocal ellipse in between, called mean or master ellipse—see the dashed ellipses in the top panels of Fig. 2a, b. As the minor and major axes of the master ellipse are given by, respectively, $2c \sinh \bar{\nu}$ and $2c \cosh \bar{\nu}$, we define the aspect ratio of a CAJTJ as $\rho \equiv \tanh \bar{\nu}$ and its (mean) eccentricity as $e^2 \equiv 1 - \rho^2 = \text{sech}^2 \bar{\nu}$.

For closely spaced inner and outer ellipses, $\Delta \nu \equiv \nu_o - \nu_i << 1$, the expression of the local annulus width is [20]:

$$\Delta w(\tau) = c \mathcal{Q}(\tau) \, \Delta \nu, \tag{1}$$

where $\mathcal{Q}(\tau)$ is the elliptic scale factor defined by $\mathcal{Q}^2(\tau) \equiv \sinh^2 \bar{\nu} \sin^2 \tau + \cosh^2 \bar{\nu} \cos^2 \tau = \sinh^2 \bar{\nu} + \cos^2 \tau = \cosh^2 \bar{\nu} - \sin^2 \tau = (\cosh 2\bar{\nu} + \cos 2\tau)/2$. The width of the confocal annulus is smallest at the equatorial points, with $\Delta w_{\min} = $

$c\Delta\nu \sinh\bar{\nu}$, and largest at the poles, with $\Delta w_{\max} = c\Delta\nu \cosh\bar{\nu}$; then, $\Delta w_{\min} = \rho\Delta w_{\max}$, i.e., interestingly, as we make the confocal annulus more eccentric we enhance the width spread $\Delta w_{\max}/\Delta w_{\min}$. This is clearly seen in Fig. 2 where the annuli are made to have the same equatorial widths, $\Delta w_{\min} = 0.1$: as we halve the aspect ratio, ρ, passing from 1/2 to 1/4, the polar width, $\Delta w_{\max}$, doubles from 0.2 to 0.4. The annuli width variations with the angular elliptic coordinate, τ, are shown in the bottom panels of Fig. 2a, b as given by (1).

In the small width approximation, $\Delta w_{\max} << \lambda_J$, where λ_J, called the Josephson penetration length, gives a measure of the distance over which significant spatial variations of the Josephson phase occur, the system becomes one dimensional. It has been derived that the ν-independent Josephson phase, $\phi(\tau, \hat{t})$, of a narrow CAJTJ in the presence of an spatially homogeneous in-plane magnetic field $\mathbf{H}$ of arbitrary orientation, $\bar{\theta}$, relative to the Y-axis, obeys a modified and perturbed sine-Gordon equation with a space-dependent effective Josephson penetration, $\lambda_J/Q(\tau)$, length inversely proportional to the local junction width [20]:

$$\left[\frac{\lambda_J}{c\,Q(\tau)}\right]^2 \left(1 + \beta\frac{\partial}{\partial\hat{t}}\right)\phi_{\tau\tau} - \phi_{\hat{t}\hat{t}} - \sin\phi = \alpha\phi_{\hat{t}} - \gamma(\tau) + F_h(\tau), \quad (2)$$

where $\hat{t}$ is the time normalized to the inverse of the so-called (maximum) plasma frequency, ω_p. The critical current density, J_c, was assumed to be uniform. The subscripts on ϕ are a shorthand for derivative with respect to the corresponding variable. Furthermore, $\gamma(\tau) = J_Z(\tau)/J_c$ is the local normalized density of the bias current and

$$F_h(\tau) \equiv h\Delta\frac{\cos\bar{\theta}\cosh\bar{\nu}\sin\tau - \sin\bar{\theta}\sinh\bar{\nu}\cos\tau}{Q^2(\tau)} \quad (3)$$

is an additional forcing term proportional to the applied magnetic field; $h \equiv H/J_c c$ is the normalized field strength for treating long CAJTJs, and Δ is a geometrical factor which sometimes has been referred to as the coupling between the external field and the flux density of the annular junction [24]. As usual, the α and β terms in (2) account for, respectively, the quasiparticle shunt loss and the surface losses in the superconducting electrodes. The perimeter of the master ellipse is $L = 4c\cosh\bar{\nu}\,\mathrm{E}(e^2)$, where $\mathrm{E}(e^2) \equiv \mathrm{E}(\pi/2, e^2)$ is the *complete* elliptic integrals of the second kind of argument e^2. Then, the normalized or electric length, $\ell = L/\lambda_J$, of the CAJTJ of a given aspect ratio grows linearly with the foci distance, $2c$.

When cooling an annular JTL below its critical temperature one or more flux quanta may be trapped in its doubly connected electrodes. The algebraic sum of the flux quanta trapped in each electrode is an integer number n, called the winding number, counting the number of Josephson vortices (fluxons) trapped in the junction barrier. To take into account the number of trapped fluxons, (2) is supplemented by periodic boundary conditions [29,30]:

$$\phi(\tau + 2\pi, \hat{t}) = \phi(\tau, \hat{t}) + 2\pi n, \quad (4a)$$

$$\phi_\tau(\tau + 2\pi, \hat{t}) = \phi_\tau(\tau, \hat{t}). \quad (4b)$$

2.1 The Single fluxon Potential

In the absence of dissipative and driving forces, the simplest topologically stable dynamic solution of (2) on an infinite line, in a first approximation, is a 2π-kink (single fluxon) centered at a time-dependent coordinate $s_0(\hat{t})$ and moving with instantaneous (tangential) velocity $\hat{u} \equiv d(s_0/\lambda_J)/d\hat{t} = (c/\lambda_J)\mathcal{Q}(\tau_0)d\tau_0/d\hat{t}$:

$$\tilde{\phi}(\tau, \hat{t}) = 4 \arctan \exp\left\{\wp[s(\tau) - s_0(\hat{t})]/\lambda_J\right\}, \tag{5}$$

where $\wp = \pm 1$ is the topological charge, i.e., the fluxon polarity [31] and $s(\tau)$ the nonlinear curvilinear coordinate $s(\tau) = c \int_0^\tau \mathcal{Q}(\tau')d\tau'$. Inserting the phase profile in (5) into (2), it was derived that [27], in the absence of external forces, the energy of a nonrelativistic fluxon ($\hat{u} \ll 1$), $\hat{E} = \hat{K} + \hat{U}_w$, is conserved. The circumflex accents denote normalized quantities. $\hat{E}$ is normalized to the characteristic energy, $\mathcal{E} = \Phi_0 J_c \lambda_J c \Delta\nu/2\pi$. Both the kinetic energy, $\hat{K}(\tau_0) \approx 4\mathcal{Q}(\tau_0)\hat{u}^2$, and the intrinsic potential energy, $\hat{U}_w(\tau_0) \approx 8\mathcal{Q}(\tau_0)$, are position dependent through the scale factor $\mathcal{Q}$, that is, in force of (1), they are proportional to the annulus width. This is consistent with the relativistic expression $\hat{E} = \hat{m}(\tau_0)/\sqrt{1 - \hat{u}^2(\tau_0)}$ reported by Nappi and Pagano [18], provided that we introduce the position-dependent reduced rest mass $\hat{m}(\tau_0) = 8\mathcal{Q}(\tau_0)$ of the fluxon. Note that the energy, E_0, of a CAJTJ containing one static vortex is $8\mathcal{E} \sinh \bar{\nu}$. With experimentally accessible geometrical and electrical parameters, the normalizing energy is much larger than $k_B T$ - $\mathcal{E} = O(10^4 K)$—and the fluxon rest mass, $m_0 \equiv E_0/\bar{c}^2$, happens to be much smaller than the electron rest mass $m_e - m_0 = O(10^{-3} m_e)$ -, where the so-called Swihart velocity [32], $\bar{c}$, is the characteristic velocity of the electromagnetic waves in JTJs.
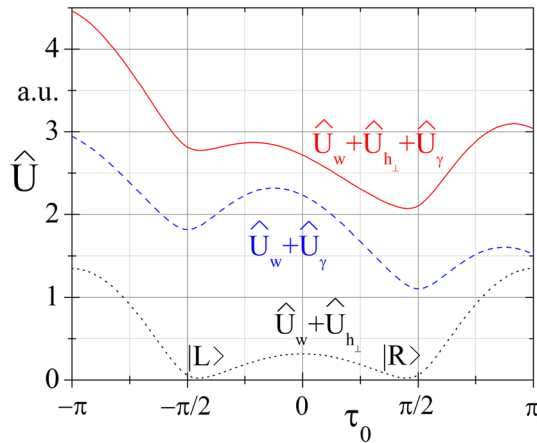
As can be discerned from the plots in the bottom panels of Fig. 2a, b, $\hat{U}_w \propto \Delta w$ expresses a π-periodic potential energy function independent on the fluxon polarity, and uniquely determined by the CAJTJ aspect ratio. The potential wells are located at $\tau_0 = \pm\pi/2$, where the confocal annulus is narrowest. The left $|L\rangle$ and right $|R\rangle$ wells of the potential constitute stable classical states for the vortex with degenerate ground state energy. Considering that $\sinh \bar{\nu} \leq \mathcal{Q}(\tau) \leq \cosh \bar{\nu}$, the potential wells are separated by a normalized energy barrier, $\Delta\hat{U}_w \equiv \hat{U}_{w,max} - \hat{U}_{w,min} = 8 \exp -\bar{\nu}$, uniquely determined by the system aspect ratio. As an example, the change in the aspect ratio from 2:1 to 4:1 in Fig. 2 results in the triplication of the energy barrier (and so of the potential gradient).

In the presence of small applied magnetic field and bias current, two more terms contribute to the total potential energy, $\hat{U}$, experienced by the fluxon:

$$\hat{U}(\tau_0) = \hat{U}_w(\tau_0) + \hat{U}_h(\tau_0) + \hat{U}_\gamma(\tau_0). \tag{6}$$

$\hat{U}_h(\tau_0)$ is the magnetic potential such that $dU_h/d\tau = 2\pi\wp(\lambda_J/c)\mathcal{Q}^2(\tau)F_h(\tau)$, i.e.,

$$\hat{U}_h(\tau_0) = \hat{U}_{h_\perp}(\tau_0) + \hat{U}_{h_\parallel}(\tau_0)$$
$$\approx 2\pi\wp(\lambda_J/c)\Delta\left(h_\perp \cosh \bar{\nu} \cos \tau_0 + h_\parallel \sinh \bar{\nu} \sin \tau_0\right),$$

Fig. 3 Schematic representation of the fluxon potential under different conditions. The dotted line at the bottom refers to the symmetric double-well potential $\hat{U}_w + \hat{U}_{h_\perp}$ in the presence of a uniform in-plane magnetic field perpendicular to the long annulus diameter with two minima at $\tau_0 \approx \pm\pi/2$ coincident with the degenerate states $|R\rangle$ and $|L\rangle$; the dashed line corresponds to $\hat{U}_w + \hat{U}_\gamma$ and displays the tilting of the potential due to a uniform bias current; the solid line shows the asymmetric potential $\hat{U}_w + \hat{U}_{h_\perp} + \hat{U}_\gamma$ in the more general case of applied (perpendicular) magnetic field and bias current. The three potentials are shifted by arbitrary vertical offsets (Color figure online)

where $h_\perp \equiv h\cos\bar{\theta}$ and $h_{||} \equiv h\sin\bar{\theta}$ are the components of the in-plane magnetic field, respectively, perpendicular and parallel to the CAJTJ's major diameter. $\hat{U}_h(\tau)$ is 2π-periodic and π-antiperiodic in τ, i.e., $\hat{U}_h(\tau + \pi) = -\hat{U}_h(\tau)$; then, it averages to zero over one period. It is important to note that $\hat{U}_{h_\perp}$ is even in τ_0 as the intrinsic potential $\hat{U}_w$, while $\hat{U}_{h_{||}}$ is odd and breaks the system parity.

Furthermore, $\hat{U}_\gamma(\tau_0)$ is the current-induced potential such that $d\hat{U}_\gamma/d\tau = 2\pi\wp(\lambda_J/c)\mathcal{Q}^2(\tau)\gamma(\tau)$, assuming a uniform current distribution $\gamma(\tau) = \gamma_0$, and it is:

$$\hat{U}_\gamma(\tau_0) \equiv \pi\wp(\lambda_J/c)\gamma_0\left(\tau_0\cosh 2\bar{\nu} + \frac{1}{2}\sin 2\tau_0\right). \tag{7}$$

Figure 3 qualitatively explains how the width-dependent fluxon potential can be tuned by means of an externally applied magnetic field and/or a bias current. The dotted curve at the bottom of Fig. 3 shows the fluxon potential in the presence of a (negative) perpendicular magnetic field $h_\perp$; the potential $\hat{U}_w + \hat{U}_{h_\perp}$ is still invariant under a parity transformation ($\tau_0 \to -\tau_0$) and develops into a field-controlled symmetric potential with finite walls and two spatially separated minima. Increasing the amplitude of the magnetic field, eventually the minima coalesce and the perturbed potential becomes single welled for a (perpendicular) threshold field strength $h_\perp^*$. The evolution of the potential $\hat{U}$ with an increasing parallel field, $h_{||}$, follows a quite different pattern (not shown in Fig. 3), but again a threshold value, $h_{||}^*$, exists where the potential $\hat{U}_w + \hat{U}_{h_{||}}$ becomes single welled. It means that the inter-well barrier can be fine-tuned and made arbitrarily small by means of both a perpendicular or a parallel in-plane magnetic field. The dashed line in Fig. 3 shows the total potential when a bias current is feeding the

CAJTJ. The resulting potential, $\hat{U}_w + \hat{U}_\gamma$, is qualitatively similar to the well-studied tilted washboard potential for the phase difference of a small JTJ biased below its critical current; the only difference is that in our case the degree of freedom is the spatial coordinate, rather than the Josephson phase difference. Indeed, the potential profile can be tilted either to left or to right depending on the polarity of the bias current, γ_0. The inclination is proportional to the Lorentz force on the vortex which is induced by the bias current applied to the junction. At last, the total fluxon potential, $\hat{U}_w + \hat{U}_{h_\perp} + \hat{U}_\gamma$, in the presence of both an applied magnetic field and bias current is depicted by the solid line at the top of Fig. 3. We note that the left well is very shallow and an increment in the bias current would further tilt the potential; a static fluxon pinned in the left well would become unstable and gets trapped in the right well as, in this specific example, it does not have enough energy to move further to the right. The smallest tilting that allows the vortex to escape from a well defines the so-called depinning current, γ_d. Clearly, the depinning current depends on the applied magnetic field and, in general, for a given field, the depinning currents, γ_d^L and γ_d^R, from the left and right wells are different. The deeper is the original potential well from which the fluxon has to escape and the larger is the corresponding depinning current.

3 The Numerical Simulations

In Fig. 4a, b we report the numerically computed field dependencies of the positive left and right depinning currents, γ_{d+}^L (open circles) and γ_{d+}^R (crosses), for a (positive) fluxon in the presence of a uniform in-plane magnetic field, respectively, parallel and perpendicular to the CAJTJ's major axis. The numerical simulations of (2) become mandatory whenever the applied bias current and/or magnetic field cannot be considered as perturbations. The commercial finite element simulation package COMSOL MULTIPHYSICS (www.comsol.com) was used to numerically solve (2) subjected to the cyclic boundary conditions in Eqs. (4a) and (4b) with $n = 1$. We set the damping coefficients $\alpha = 0.05$ to simulate a weakly underdamped regime and $\beta = 0$ as we are considering quasi-static phase solutions. We assumed a uniform current distribution, i.e., $\gamma(\tau) = \gamma_0$. In addition, the field coupling constant, Δ, was set equal to 1. In order to compare the numerical results with the experimental findings presented in the next section, we set the annulus aspect ratio to $\rho = 1/4$ corresponding to a CAJTJ whose largest width is four times larger than the smallest one—as depicted in Fig. 2b. Furthermore, the normalized length, $\ell = L/\lambda_J$, was set to be 10π; then, the (smooth) variation of the annulus width occurs over a length, $L/4 = 2.5\pi\lambda_J \approx 8\lambda_J$, quite large compared to the fluxon size. A static fluxon centered either in the left ($\tau_0 = -\pi/2$) or right well ($\tau_0 = \pi/2$) was chosen for the system initial condition with $\gamma_0 = 0$ in (2); then, the normalized bias current was ramped-up in small adiabatic increments of 0.05 and the stationary, i.e., time-independent solutions recorded until the fluxon was depinned from its initial state.

We first note that the field dependencies of the depinning current shown in Fig. 4a, b are qualitatively similar despite the quite different ways the parallel and perpendicular fields affect the fluxon potential. The most evident discrepancy resides in the magnetic scales and reflects the fact that the junction cross section seen by a perpendicular
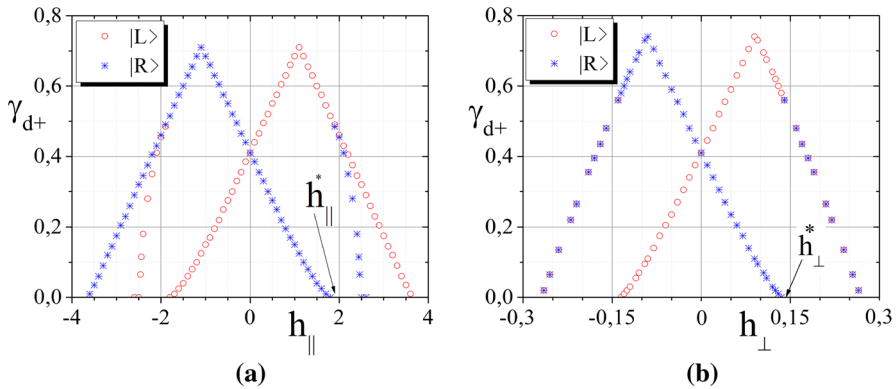
Fig. 4 Numerically computed field dependencies of the positive fluxon depinning currents of the $|L\rangle$ (open circles for γ_{d+}^L) and $|R\rangle$ (stars for γ_{d+}^R) states for two values of the in-plane field orientation with respect to the annulus major axis: **a** parallel field, $h_{||}$, and **b** perpendicular field, $h_\perp$. The magnetic fields are normalized to $J_c c$ (Color figure online)

field is larger than its parallel counterpart [33,34]. In both cases, the exchange of the fluxon initial position is equivalent to a field reversal, i.e., $\gamma_{d+}^L(h_{||}) = \gamma_{d+}^R(-h_{||})$ and $\gamma_{d+}^L(h_\perp) = \gamma_{d+}^R(-h_\perp)$. As expected, the zero-field depinning currents are degenerate, $\gamma_{d+}^L(0) = \gamma_{d+}^R(0)$, and constitute an appreciable fraction, that is 41%, of the zero-field critical current; a smaller value, that is 19%, has been reported [28] for a CAJTJ with aspect ratio $\rho = 1/2$. These different values reflect the fact that the deeper is the potential well and the largest is the bias current needed to unpin the fluxon. As a parallel magnetic field is turned on, it is seen from Fig. 4a that the left and right depinning currents change quite linearly and in opposite directions, as long as the amplitude of the applied field is smaller than a characteristic field value $h_{||}^*$ where one of the depinning currents vanishes. In other words, for $|h_{||}| \leq h_{||}^*$ the fluxon escape from the $|L\rangle$ and $|R\rangle$ states occurs at quite different bias currents. The state with the higher depinning current corresponds to a deeper potential well when the CAJTJ is unbiased; numerical simulations show that when the fluxon escapes from the state with higher depinning current it starts to travel along the annulus perimeter and switches the junction into a dynamic state with a finite voltage across the junction proportional to the fluxon time-averaged speed. Therefore, in this particular case, the depinning current identifies with the switching current that can be easily determined experimentally. This is not necessarily the case for the state with lower depinning current, as it might happen that, once depinned, the fluxon gets trapped in the opposite well which has an higher depinning current [35], so that the junction remains in a time-independent, i.e., zero-voltage, state. Numerical analysis shows that this situation only occurs for magnetic fields whose absolute values are close to—but lower than—$h_{||}^*$. Furthermore, the re-trapping drastically depends on the junction losses that may dissipate the energy of the depinned fluxon well before it overcomes the opposite well. When the loss parameter α in (2) is decreased to 0.01, the re-trapping field range shrinks, but does not vanish; therefore, even lower losses should be used in the numerical analysis to investigate the re-trapping conditions. However, great care

must be taken to simulate low-damping nonlinear systems, since, besides the longer transients, the results are very sensitive to the numerical algorithm adopted to integrate the partial differential equation. Nevertheless, setting $\alpha = 0.05$ the fluxon escaping from the state with the lower depinning range jumps over the opposite well and enters the running mode in a field range of approximately $|h_{||}| \leq h_{||}^*/2$. In this range, we can talk again of a switching current that coincides with the depinning current. We recall that in the experiments with high-quality JTJs the losses drastically decrease with the temperature [36] and it is not difficult to reach damping parameters as small as 0.001 [37]. Notably, the existence of a range of parallel fields in which also the lower depinning current turns the CAJTJ into a finite voltage state implies that a switching current measurement [38] allows to localize the vortex in one of the two states. (This technique has been successfully used to prove the existence of a DWP in other Josephson vortex qubit prototypes [14,35,39].) As $|h_{||}|$ exceeds $h_{||}^*$ the unbiased fluxon potential becomes single welled, the information about the vortex initial state is lost, and the left and right depinning currents suddenly coincide. At this point, an eventual reduction of the field amplitude below $h_{||}^*$ and even its full removal leaves the fluxon in the left or in the right well depending on its original sign; in different words, the proper ramping up and down of just the parallel field represents a viable procedure to prepare the vortex state. Similar considerations also apply to the case of a perpendicular magnetic field; the only significant difference is that the preparation of the fluxon state, beside a magnetic field $|h_\perp| > h_\perp^*$, also requires a small bias current that breaks the system symmetry [40].

4 The Measurements

In this section, we report on the switching currents measured on high-quality window-type Nb/Al-AlO$_x$-Al/Nb CAJTJs with a single fluxon trapped during the zero-field cooling of the samples through their critical temperature, $T_c \approx 9.2$ K. This process is known to spontaneously generated one or more fluxons on a statistical basis [41,42] with a probability that increases with the speed of the normal-to-superconducting transition; at the end of each quench, the number of trapped fluxons is determined by carefully inspecting the junction current-voltage characteristic (IVC) and measuring the voltage of possible current branches, the so-called *zero-field steps*, associated with the traveling of the Josephson vortices around the annulus. The samples designed to test the theory had the so-called *Lyngby-type* geometry [21] that refers to a specularly symmetric configuration, as that shown in Fig. 1, in which the width of the current carrying electrodes matches one of the axes of the outer ellipse and the tunneling area is obtained by the superposition of two superconducting rings. More details on the samples description and their fabrication were reported, respectively, in Ref.[28] and Ref.[43]. Some electrical parameters (measured at 4.2 K) and the geometrical details of the tunneling area for our CAJTJs are listed in Table 1. The samples normalized length is $L/\lambda_J \approx 32.2 \approx 10\pi$. We observe that the annulus polar width, Δw_{max}, slightly exceeds the fluxon size, λ_J, meaning that the samples are not strictly one dimensional. In addition, the smallest curvature radius of the master ellipse occurring at the equatorial points, $c\rho \sinh \bar{\nu} \approx 2.9\,\mu$m, is smaller than the fluxon size, a fact that

Table 1 Some electrical parameters (at 4.2 K) of our CAJTJs and the geometrical details of their tunneling area

J_c (kA/cm^2)	λ_J (μm)	ρ	$\bar{\nu}$	$\Delta\nu$	c (μm)	Δw_{min} (μm)	Δw_{max} (μm)	A (μm^2)	L (μm)
1.1	6.2	0.25	0.256	0.18	45.1	2.1	8.4	1310	200
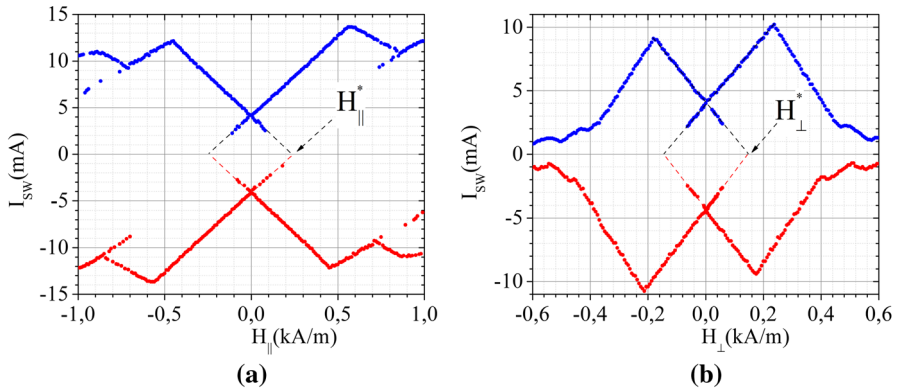
Fig. 5 Positive and negative switching currents, I_{SW}, recorded at $T = 4.2$ K, by continuously sweeping the bias current as an in-plane magnetic field is changed; the dashed lines are the extrapolations of the almost linear branches that help to locate the threshold field $H^*_{\parallel,\perp}$; **a** parallel field, $H_{\parallel}$, and **b** perpendicular field, $H_{\perp}$ (Color figure online)

may induce an interaction (repulsion) between the leading and trailing edges of the fluxon.

Several nominally identical CAJTJs fabricated on different chips within the same run of a standard Nb–AlO$_x$–Nb trilayer process were investigated. Their electrodes were either parallel, as shown in Fig. 1, or perpendicular to the annulus major diameter, and they all gave qualitatively similar results regardless of the orientation of the bias. More important was found to be the orientation of the externally applied in-plane magnetic field; in Fig. 5a, b, we report the field dependence of the positive and negative switching currents measured at $T = 4.2$ K on two representative samples subject to in-plane magnetic fields having orthogonal orientations, respectively, $H_{\parallel}$ and $H_{\perp}$. The switching currents, I_{SW}, were obtained by continuously sweeping the bias current with a sufficiently large symmetric triangular waveform with a frequency of few hertz and automatically recording the largest (and smallest) zero-voltage current ten times for each value of the externally applied magnetic field. In agreement with the numerical expectations presented in the previous section, in a field range centered around zero, the switching current was found to be double valued. This is a clear indication that the fluxon experiences a potential profile with two stable states and, when the sweeping current crosses zero, the decelerating fluxon stops on a statistical basis in either one of the two different-depth potential wells. The pinning process of a particle slowing down in a DWP drastically depends on the drag force experienced by the particle; in fact, by repeating the measurements at different temperatures, the double-valued field range progressively shrank as the temperature, and so the losses, was increased.

Higher temperatures also means larger thermal fluctuations that might induce hopping between the two states. Other noise sources, such as current and/or field noise, concur on limiting the field range of the fluxon state having the lower switching current; in fact, few more values of the magnetic field were found to show a double-valued switching current using a manual battery-operated ramping of the bias current. The moderate skewness of the switching current plots is ascribed to fact that for both samples the bias current flow occurs in the direction orthogonal to the applied field [44]; in this configuration, the self-field adds to the external field in the second and fourth quadrants, while in the first and third quadrants it partially compensates the applied field. We found the switching current field dependence to be quite linear and the dashed lines in Fig. 5a, b are the linear extrapolations that help to locate the threshold field $H^*_{||,\perp}$, i.e., the largest theoretical absolute value of the field that would yield a double-valued switching current whenever both the dissipation and noises can be neglected. Therefore, according to our measurements, the determination of the fluxon state can be reliably achieved by applying to an unbiased CAJTJ an in-plane magnetic field that is known to have quite different switching currents for the two states and then incrementing the bias current with a constant rate until a sudden jump of the voltage from zero to any finite value is detected.

It is worthwhile to mention that the finite voltage observed after a switch does not necessarily have to be $v\Phi_0/L$ corresponding to the fluxon continuous motion along the annulus perimeter, L, with a certain time-averaged speed v. In most cases, the junction switched to a state of free-running phase on the McCumber curve, i.e., at a voltage close to the junction gap voltage $V_g \approx 2.8\,\text{mV}$, in particular when the switch occurred from the state with the higher switching current. It means that the fluxon potential is too *steep* to allow a steady motion; in fact, as the numerical analysis shows, the plasma waves emitted by the leading (trailing) edge of the accelerating (decelerating) fluxon might grow in size as far as they break in a fluxon–antifluxon pair; the process of pair nucleation continues until the system becomes unstable [45]. Beside the potential gradient, this radiative process heavily depends on several factors, such as the fluxon speed and the annulus perimeter, but again, above all it is determined by the system dissipation. Indeed, for the high aspect-ratio CAJTJs considered in this paper, temperatures larger than $T = 4.2\,\text{K}$ were needed to observe the zero field steps. This fact indicates that, as the system losses are increased, for a given bias current, the fluxon average speed gets smaller; in turn, the emitted plasma waves not only have a smaller amplitude but also die away faster and then the conditions are restored for a regular stable motion of the fluxon.

5 Conclusion

A Josephson vortex trapped in an long and narrow CAJTJ in the presence of an in-plane magnetic field is subjected to a periodic asymmetric and fine-tunable double-well potential accurately modeled by a modified and perturbed one-dimensional sine-Gordon equation. The key ingredient of this potential is the smoothly distributed modulation of the planar tunnel barrier width whose gradient is related one-to-one to the eccentricity of the elliptical annulus. Numerical simulations and experiments car-

ried on high-quality Nb/Al-AlO$_x$-Al/Nb samples with one trapped fluxon demonstrate that a robust two-minima potential can be tailored whose inter-well barrier grows as the annulus is made more eccentric. We have found that the depinning of the fluxon occurs at a bias current that, among other things, depends on the potential well from which the fluxon is escaping. We considered uniform magnetic fields applied in the barrier plane either perpendicular or parallel to the major axis of the CAJTJ. In both cases, although for different reasons, a wide range of magnetic field was observed characterized by two-valued depinning currents, each value corresponding to either one of the potential stable states. Experiments carried out on CAJTJs with an aspect ratio of 4:1 indicate that these ranges grow as the temperature decreases, and so the fluxon losses, and/or as the noise sources are reduced.

The eccentricity of a CAJTJ also has a drastic effect on the motion of a fluxon whose total energy exceeds the potential energy. In fact, as the aspect ratio is increased, the growing accelerations and decelerations the traveling fluxon experiences when it approaches the region of, respectively, smallest and larger width are responsible of a periodic radiation of small amplitude waves that destabilize the forward fluxon advancement. Both numerical simulations and experiments with slightly damped CAJTJs having an aspect ratio of 4:1 showed no manifestation of the fluxon propagation along the annulus perimeter.

Despite all the above considerations, we observed that the eccentricity of the CAJTJs does not affect the robustness and reliability of the operation of a CAJTJ as a Josephson vortex two-state system. Only small quantitative differences were observed in the depinning currents of samples with different aspect ratios. In conclusion, we have demonstrated the full reliability of the procedures for both the preparation and the determination of the vortex in either one of the two potential minima, that are important for the possible realization of a vortex qubit.

References

1. F. Hund, Significance of molecular spectra. III. Notes on the oscillation and rotation spectra of molecules with more than two nuclei. Z. Phys. **43**, 805 (1927)
2. M.D. Dennison, G.E. Uhlenbeck, The two-minima problem and the ammonia molecule. Phys. Rev. **41**, 313 (1932)
3. E.L. Levy, I. Shomroni, J. Steinhauer, The a.c. and d.c. Josephson effects in a Bose–Einstein condensate. Nature **449**, 579 (2007)
4. T. Anker, M. Albiez, R. Gati, S. Hunsmann, B. Eiermann, A. Trombettoni, M.K. Oberthaler, Nonlinear self-trapping of matter waves in periodic potentials. Phys. Rev. Lett. **94**, 020403 (2005)
5. M. Albiez, R. Gati, J. Folling, S. Hunsmann, M. Cristiani, M.K. Oberthaler, Direct observation of tunneling and nonlinear self-trapping in a single bosonic Josephson junction. Phys. Rev. Lett. **95**, 010402 (2005)
6. Y. Shin, G.B. Jo, M. Saba, T.A. Pasquini, W. Ketterle, D.E. Pritchard, Optical weak link between two spatially separated Bose–Einstein condensates. Phys. Rev. Lett. **95**, 170402 (2005)
7. B.V. Hall, S. Whitlock, R. Anderson, P. Hannaford, A.I. Sidorov, Condensate splitting in an asymmetric double well for atom chip based sensors. Phys. Rev. Lett. **98**, 030402 (2007)

8. Y. Makhlin, G. Schön, A. Shnirman, Josephson-junction qubits with controlled couplings. Nature **398**, 305 (1999)
9. J.E. Mooij, T.P. Orlando, L. Levitov, T. Tian, C.H. van derWal, S. Lloyd, Josephson persistent-current qubit. Nature **285**, 1036 (1999)
10. J.R. Friedman, V. Patel, W. Chen, S.K. Tolpygo, J.E. Lukens, Quantum superposition of distinct macroscopic states. Science **406**, 43 (2000)
11. J.Q. You, J.S. Tsai, F. Nori, Scalable quantum computing with Josephson charge qubits. Phys. Rev. Lett. **89**, 197902 (2002)
12. Y. Yu, S.Y. Han, X. Chu, S.I. Chu, Z. Wang, Coherent temporal oscillations of macroscopic quantum states in a Josephson junction. Science **296**, 889 (2002)
13. A. Wallraff, Y. Koval, M. Levitchev, M.V. Fistul, A.V. Ustinov, Annular long Josephson junctions in a magnetic field: engineering and probing the fluxon interaction potential. J. Low Temp. Phys. **118**, 543 (2000)
14. A. Wallraff, A. Lukashenko, J. Lisenfeld, A. Kemp, M.V. Fistul, Y. Koval, A.V. Ustinov, Quantum dynamics of a single vortex. Nature **425**, 155 (2003)
15. T. Kato, M. Imada, Macroscopic quantum tunneling of a fluxon in a long Josephson junction. J. Phys. Soc. Jpn. **64**, 2963 (1996)
16. J.H. Kim, R.P. Dhungana, K.-S. Park, Decoherence in Josephson vortex quantum bits: Long-Josephson-junction approach to a two-state system. Phys. Rev. B **73**, 214506 (2006)
17. E. Goldobin, A. Sterck, D. Koelle, Josephson vortex in a ratchet potential: theory. Phys. Rev. E **63**, 031111 (2001)
18. C. Nappi, S. Pagano, Fluxon dynamics in non uniform width Josephson transmission lines, in *National Workshop on Nonlinear Dynamics*, ed. by M. Costato, A. Degasperis, M. Milani (Italian Physical Society, Bologna, 1995), p. 261
19. A. Benabdallah, J.G. Caputo, A.C. Scott, Exponentially tapered Josephson flux-flow oscillator. Phys. Rev. B **54**, 16139 (1996)
20. R. Monaco, Confocal annular Josephson tunnel junctions. J. Low Temp. Phys. **184**, 979 (2016)
21. A. Davidson, B. Dueholm, B. Kryger, N.F. Pedersen, Experimental investigation of trapped sine-Gordon solitons. Phys. Rev. Lett. **55**, 2059 (1985)
22. A. Davidson, B. Dueholm, N.F. Pedersen, Experiments on soliton motion in annular Josephson-junctions. J. Appl. Phys. **60**, 1447 (1986)
23. A.V. Ustinov, T. Doderer, R.P. Huebener, N.F. Pedersen, B. Mayer, V.A. Oboznov, Dynamics of sine-Gordon solitons in the annular Josephson junction. Phys. Rev. Lett. **69**, 1815 (1992)
24. N. Grönbech-Jensen, P.S. Lomdahl, M.R. Samuelsen, Phase-locking of long annular Josephson-junctions coupled to an external RF magnetic-field. Phys. Lett. A **154**, 14 (1991)
25. A.V. Ustinov, Observation of a radiation-induced soliton resonance in a Josephson ring. JETP Lett. **64**, 191 (1996)
26. N. Martucciello, J. Mygind, V.P. Koshelets, A.V. Shchukin, L.V. Filippenko, R. Monaco, Fluxon dynamics in long annular Josephson tunnel junctions. Phys. Rev. B **57**, 5444 (1998)
27. R. Monaco, Engineering double-well potentials with variable-width annular Josephson tunnel junctions. J. Phys. Condens. Matter **28**, 445702 (2016)
28. R. Monaco, J. Mygind, V.P. Koshelets, Development of a Josephson vortex twostate system based on a confocal annular Josephson junction. Supercond. Sci. Technol. **31**, 025003 (2018)
29. N. Martucciello, R. Monaco, Annular Josephson tunnel junctions in an external magnetic field: the statics. Phys. Rev. B **53**, 3471 (1996)
30. N. Martucciello, C. Soriano, R. Monaco, Annular Josephson tunnel junctions in an external magnetic field: the dynamics. Phys. Rev. B **55**, 15157 (1997)
31. D.W. McLaughlin, A.C. Scott, Perturbation analysis of fluxon dynamics. Phys. Rev. A **18**, 1652 (1978)
32. J.C. Swihart, Field solution for a thin-film superconducting strip transmission line. J. Appl. Phys. **21**, 461–469 (1961)
33. R.L. Peterson, J.W. Ekin, Critical-current diffraction patterns of grain-boundary Josephson weak links. Phys. Rev. B **42**, 8014 (1990)
34. C. Nappi, R. Monaco, Critical current diffraction pattern of elliptic annular Josephson tunnel junctions. Physica C **520**, 36 (2016)
35. G. Carapella, F. Russo, R. Latempa, G. Costabile, Preparation and readout of a Josephson vortex in a double-well potential. Phys. Rev. B **70**, 092502 (2004)

36. R. Cristiano, L. Frunzio, R. Monaco, C. Nappi, S. Pagano, Investigation of subgap structures in high-quality Nb/AlOx/Nb tunnel-junctions. Phys. Rev. B **49**, 429 (1994)

37. N.F. Pedersen, D. Welner, Analytical results for the fluxon-antifluxon annihilation process in Josephson-junctions. Phys. Rev. B **29**, 2551 (1985)

38. M. Lisitskiy, D. Massarotti, L. Galletti, L. Longobardi, G. Rotoli, M. Russo, F. Tafuri, B. Ruggiero, Bias current ramp rate dependence of the crossover temperature from Kramers to phase diffusion switching in moderately damped NbN/AlN/NbN Josephson junctions. J. Appl. Phys. **116**, 043905 (2014)

39. A.N. Price, A. Kemp, D.R. Gulevich, F.V. Kusmartsev, A.V. Ustinov, Vortex qubit based on an annular Josephson junction containing a microshort. Phys. Rev. B **81**, 014506 (2010)

40. A fluxon can be depinned by both a positive or a negative bias current; for the negative depinning currents, $\gamma_{d-}^{L,R}$, it was found that $\gamma_{d-}(h_{||}) = -\gamma_{d+}(-h_{||})$ and $\gamma_{d-}(h_\perp) = -\gamma_{d+}(h_\perp)$. It follows that the determination of the fluxon state can also be accomplished through the measurement of a negative current switch

41. R. Monaco, M. Aaroe, J. Mygind, R.J. Rivers, V.P. Koshelets, Experiments on spontaneous vortex formation in Josephson tunnel junctions. Phys. Rev. B **74**, 144513 (2006)

42. R. Monaco, M. Aaroe, J. Mygind, R.J. Rivers, V.P. Koshelets, Spontaneous fluxon production in annular Josephson tunnel junctions in the presence of a magnetic field. Phys. Rev. B **77**, 054509 (2008)

43. L.V. Filippenko, S.V. Shitov, P.N. Dmitriev, A.B. Ermakov, V.P. Koshelets, J.R. Gao, Integrated superconducting receiver: fabrication and yield. IEEE Trans. Appl. Supercond. **11**, 816 (2001)

44. R. Monaco, V.P. Koshelets, A. Mukhortova, J. Mygind, Self-field effects in window-type Josephson tunnel junctions. Supercond. Sci. Technol. **26**, 055021 (2013)

45. S. Pagano, M.P. Soerensen, P.L. Christiansen, R.D. Parmentier, Stability of fluxon motion in long Josephson-junctions at high bias. Phys. Rev. B **38**, 4677 (1988)